A theory of rupture pulse on softening interface with application to the Chi-Chi earthquake

Alexander M. Linkov[1,2]

Received 9 June 2005; accepted 11 April 2006; published 19 September 2006.

[1] The rupture process at the near-front zone of a propagating crack, being strongly nonlinear and irreversible, a detailed Fourier analysis becomes complicated, often impractical. Meanwhile, a simplified approach, employing formally derived dispersion equation, may serve for obtaining meaningful information. Data on the rupture velocity, the size of the fracture process zone (FPZ), the possibility of exponential growth in time, and also on decaying with the distance from the rupture surface become available. The approach actually presumes that the size of the FPZ defines a dominant wavelength in the Fourier spectrum of a propagating rupture pulse. We verify this suggestion by revisiting the classical problem of a propagating shear crack having a cohesive FPZ with linear softening. It appears that in this particular problem, the simplified approach provides results which remarkably agree with the exact solution. This suggests using the approach for the analysis of the unique data on a rupture pulse obtained in the Chi-Chi (Taiwan, 20 September 1999) earthquake. We conclude that the approach allows easy interpretation of the observed phenomena. The importance of the softening modulus as an independent characteristic of initiation and propagation of rupture is emphasized.

Citation: Linkov, A. M. (2006), A theory of rupture pulse on softening interface with application to the Chi-Chi earthquake, *J. Geophys. Res.*, *111*, B09307, doi:10.1029/2005JB003880.

1. Introduction

[2] In the earthquake science, the analytical and numerical study of a propagating crack having a small slip-weakening fracture process zone (FPZ) started some 30 years ago [*Ida*, 1972; *Andrews*, 1976; *Burridge et al.*, 1979; *Rice*, 1980]. Recently, the unique near-field recordings in the Chi-Chi (Taiwan, 1999) earthquake clearly revealed the so-called conspicuous S_1 phase "associated with the rupture pulse" [*Chen et al.*, 2001, p. 1251]. This earthquake gave rise to a number of new numerical simulations of a propagating pulse with slip weakening in the FPZ [e.g., *Dalguer et al.*, 2001; *Oglesby and Day*, 2001].

[3] These investigations explicitly accounted for the effect of contact weakening, that is decreasing of the cohesive strength with growing displacement discontinuity (DD) at the crack surface in the FPZ (Figure 1a). In mining geomechanics, such behavior, called postfailure deformation or softening, also has been a subject of many researches [e.g., *Cook*, 1965; *Crouch and Fairhurst*, 1974; *Barton and Chaubey*, 1977; *Linkov*, 1978, 1994; *Petukhov and Linkov*, 1979; *Ohnaka and Kuwahara*, 1990]. It is characterized by the softening modulus M. For softening at surfaces its dimension is [stress/length]. Commonly, the simplest piecewise approximation (Figure 1b), neglecting ascending elastic portion of a diagram, is used [e.g., *Ida*, 1972; *Andrews*, 1976, 1985; *Burridge et al.*, 1979; *Linkov*, 1978, 1994, 2005; *Petukhov and Linkov*, 1979; *Day*, 1982, *Olsen et al.*, 1997; *Fukuyama and Madariaga*, 1998; *Harris and Day*, 1999; *Dalguer et al.*, 2001].

[4] Two features of the softening behavior, as any plastic deformation, strongly complicate an analysis: (1) nonlinearity, which in the considered case appears in the change of the softening modulus to zero at the residual strength and (2) irreversibility, which makes deformations path-dependent and, in particular, prevents restoring the strength when the DD are reversed; the reversion leads to elastic unloading of a surface (lines AC in Figures 1a and 1b). The alternative, active plastic deformation (AB) or elastic unloading (AC) at each point of the postpeak curve, presents a significant difference with the elastic interaction of surfaces (Figure 1c), for which increasing and decreasing increments of the DD follow the same diagram.

[5] The first of the features leads to the residual strength (horizontal portions in Figures 1a and 1b). The points where the residual strength is reached, become points of the newly produced crack surface. Hence the size of the FPZ is defined by the condition that the strength has decreased to its residual value. The second feature, irreversibility, has not influenced previous studies by *Ida* [1972], *Andrews* [1976, 1985], *Burridge et al.* [1979], *Dalguer et al.* [2001], and other researchers, since they assumed that in a real earthquake the DD in the FPZ only grow.

[1]Institute for Problems of Mechanical Engineering, Russian Academy of Sciences, St. Petersburg, Russia.
[2]Now at Department of Mathematics, Rzeszow University of Technology, Rzeszow, Poland.

0148-0227/06/2005JB003880$09.00

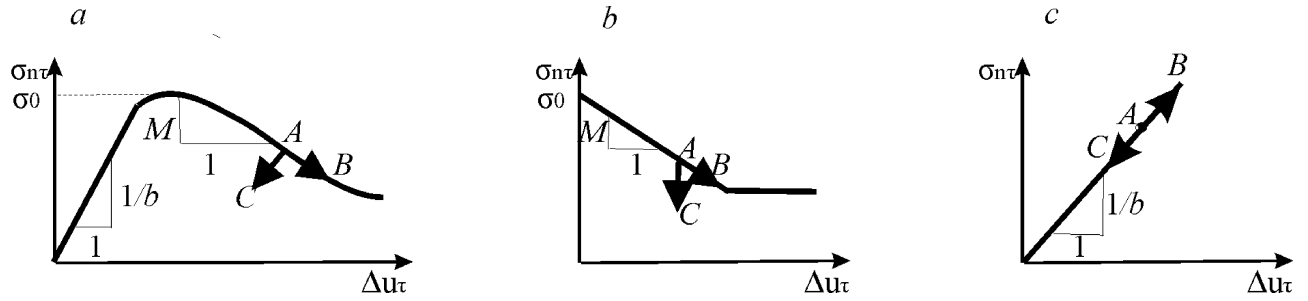

Figure 1. Diagrams of contact interaction: (a) complete diagram; (b) piecewise linear approximation; and (c) diagram of elastic interaction.

[6] However, the second, as well as the first feature, becomes crucial when trying to use harmonic analysis: In a harmonic cycle, the DD periodically change the sign, what makes the softening portions of the diagrams inapplicable. Hence, in contrast with reversible elastic interaction of surfaces (Figure 1c), studied by *Pyrak-Nolte and Cook* [1987], we cannot consider a harmonic oscillation of a single fixed frequency propagating along a softening contact. A propagating rupture pulse is represented by an infinite set of harmonics, each of which, strictly speaking, has no physical significance.

[7] Still, the length of the FPZ has to reveal itself in the Fourier spectrum; for a rupture pulse, it will define a dominant wavelength. Thus we may expect that a single harmonic wave with a properly chosen wavelength contains physically significant information on the rupture pulse. If a success, we may formally extend results obtained for elastic contacts to softening contacts.

[8] An approach to distinguish a single harmonic, containing the information on the FPZ, may be as follows. We assume linear softening (Figure 1b) and neglect irreversibility. Then a problem becomes similar to that for an elastic contact, but with negative contact rigidity. The formal similarity allows one easily to derive a dispersion equation, which connects the complex frequency with the velocity of the rupture propagation. The imaginary part of the frequency characterizes the needed wavelength. It is closely related to the size of the FPZ. It also defines the distance from the interface, at which the pulse may be recorded. The character of the dispersion (normal, when the wavelength grows with increasing velocity, or abnormal) may serve for conclusions on the stability of the propagation. The real part of the frequency characterizes the exponential growth or decaying of the DD at the end of the FPZ. Thus the approach may serve as a simple tool for at least rough estimations of a propagating rupture pulse. It easily accounts for the difference in the elastic moduli of media, viscosity of a contact, the angle of contact friction and also interaction between the modes of rupture.

[9] This makes reasonable to examine to what extent the approach is applicable quantitatively. The paper aims to obtain an answer by considering a particular case having analytical solution. We revisit the scheme of the propagating mode II shear crack with softening in the FPZ [*Burridge et al.*, 1979]. It appears that in this case, the results of the approach remarkably agree with the exact solution, especially for the subsonic crack propagation. This serves for the analysis of the subsonic rupture pulse recorded in the Chi-Chi earthquake.

[10] Appendix A contains a summary of the dispersion equations, which may serve when employing the approximate approach. The equations account for the difference in elastic moduli of half-spaces, viscosity of the interface, the angle of contact friction and interaction between the rupture modes.

[11] Note that in contrast with a pulse propagating along an interface, the irreversibility does not present a real difficulty when studying reflected and transmitted waves generated by incident waves at a softening surface. In this case, one may follow increments of waves by solving ordinary differential equations [e.g., *Linkov and Durrheim*, 1998; *Linkov*, 2001].

2. Problem Formulation and Solution

2.1. Problem Formulation

[12] Consider a shear rupture zone propagating with the velocity v in the direction of the x axis (Figure 2). Assume that the properties of the media 1 and 2 are the same. The size a of the FPZ is small as compared with the total size of the rupture surface; the external driving forces are remote. We assume also that the velocity does not change significantly at the propagation distance of order a. Under these assumptions, the crack may be considered semi-infinite and its movement steady. The latter allows us to consider

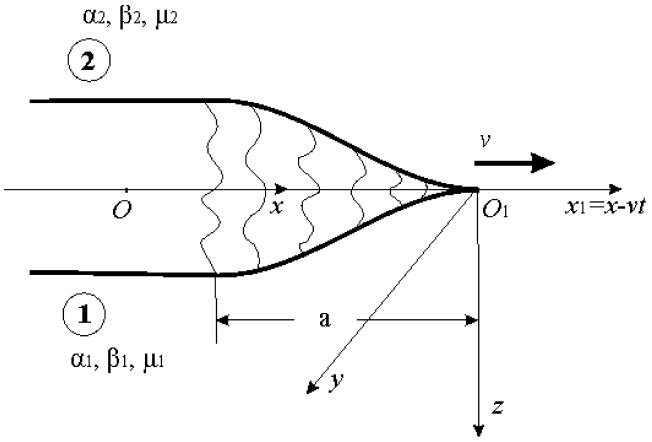

Figure 2. Coordinate system (x_1, y, z) moving with the velocity v along the interface of half-spaces.

displacements and tractions in and around the FPZ to be functions of $q = t - px$, where $p = 1/v$ is the slowness.

[13] We apply the Fourier transform defined as

$$f(\omega) = \int_{-\infty}^{\infty} f(q)\exp(-i\omega q)dq, \tag{1}$$

so that its inversion is

$$f(q) = \frac{1}{2\pi}\int_{-\infty}^{\infty} f(\omega)\exp(i\omega q)d\omega. \tag{2}$$

[14] Equations of dynamic plane strain elasticity are satisfied for media 1 and 2 by using scalar and vector potentials [see, e.g., *Aki and Richards*, 1960; *Slepyan*, 2002] of the argument q. Then, omitting details of routine derivations [e.g., *Linkov*, 2001], in the case of continuous tractions σ_{zz}, σ_{zx} and continuous normal component u_z of displacements, we arrive at the dependence between the Fourier images of the shear traction $\sigma_{zx}(\omega)$, and the shear DD $\Delta u_x(\omega) = u_{x1}(\omega) - u_{x2}(\omega)$ at $z = 0$:

$$\frac{d\Delta u_x}{dx_1}(k_w) = \frac{1}{p\mu}C\sigma_{zx}(k_w), \tag{3}$$

where $C = 2p\beta\varsigma_\beta/\Delta_R$, β is the shear wave velocity ($\beta = \sqrt{\mu/\rho}$); $\Delta_R = 4\frac{\beta}{\alpha}p^2\beta_\beta^2\zeta_\beta\zeta_\alpha + (2p^2\beta^2 - 1)^2$,

$$\zeta_\beta = -i\mathrm{sgn}\omega\sqrt{p^2\beta^2 - 1} \qquad v < \beta,$$

$$\zeta_\beta = \sqrt{1 - p^2\beta^2} \qquad v > \beta,$$

$$\zeta_\alpha = -i\mathrm{sgn}\omega\sqrt{p^2\alpha^2 - 1}, \tag{4}$$

α is the longitudinal wave velocity ($\alpha = \sqrt{(2-2\nu)/(1-2\nu)}\beta$), ν is the Poisson's ratio. The definitions of ζ_β and ζ_α are such that a solution does not tend to infinity when $|z| \to \infty$.

[15] In terms of the derivative of the DD with respect to the coordinate $x_1 = x - vt$, moving with the velocity $v = 1/p$, and the Fourier transform with respect to x_1, (3) becomes

$$\frac{d\Delta u_x}{dx_1}(k_w) = \frac{1}{\mu}C\sigma_{zx}(k_w), \tag{5}$$

with the change $k_w = -\omega p$, so that $\mathrm{sgn}\omega = -\mathrm{sgn}k_w$ in the definitions (4).

[16] Note that the absolute value $|C|$ does not depend on the parameter of the Fourier transform. Hence it is reasonable to represent C as $C = |C(v)|\exp(-i\pi\gamma\,\mathrm{sgn}k_w)$, where $\gamma = \gamma(v)$ also does not depend on the parameter of the Fourier transform:

$$\gamma = \begin{cases} 0.5, & v < v_R \\ -0.5, & v_R < v < \beta \\ \dfrac{1}{\pi}\arctan\dfrac{4\frac{\beta}{\alpha}p^2\beta^2\sqrt{1-p^2\beta^2}\sqrt{p^2\alpha^2-1}}{\left(2p^2\beta^2-1\right)^2} & \beta < v < \alpha, \end{cases} \tag{6}$$

v_R is the Rayleigh wave velocity defined by the equation $\Delta_R = 0$. Then (5) becomes

$$\frac{d\Delta u_x}{dx_1}(k_w) = \frac{1}{\mu}|C(v)|\exp(-i\pi\gamma\mathrm{sgn}k_w)\sigma_{zx}(k_w). \tag{7}$$

When $\gamma = 0.5$, what in view of (6) occurs is the case when either $v < v_R$ (in the entire subsonic region) or $v = \sqrt{2}\beta$ (in the intersonic region), the inversion of (7) is straightforward: It is obtained by applying the convolution theorem [see, e.g., *Korn and Korn*, 1968]. The result is

$$-\frac{d\Delta u_x(x_1)}{dx_1} = \frac{1}{\pi\mu}|C(v)|\int_{-\infty}^{\infty}\frac{\sigma_{zx}(\eta)}{\eta - x_1}d\eta.$$

This was obtained by *Galin* [1953] for steady subsonic crack propagation. In the static case ($v = 0$), it turns into the well-known equation [e.g., *Muskhelishvili*, 1975] with $C = 2(1 - \nu)$. This implies that results for a static problem are true for a dynamic problem when $\gamma = 0.5$ with the only change $|C(0)|$ to $|C(v)|$.

[17] So far, we have employed three of four boundary conditions at $z = 0$: the continuity of tractions and normal component of displacements at the entire axis $-\infty < x_1 < \infty$. Now we specify the conditions for the shear DD and tractions. We assume that there is no shear displacement discontinuity ahead of the crack tip, that is,

$$\Delta u_x(x_1) = 0 \text{ for } x_1 \geq 0. \tag{8}$$

[18] Behind the tip, in the FPZ ($-a \leq x_1 \leq 0$), the dependence between the shear DD and the shear traction is defined by a softening law. For simplicity, we assume the common diagram shown in Figure 1b. Without loss of generality, its horizontal portion may be assumed coinciding with the abscissa: Because of the superposition principle, this simplification influences only external loads. Then

$$\sigma_{zx} = \begin{cases} \sigma_0 - M\Delta u_x & 0 \leq \Delta u_x \leq \sigma_0/M \\ 0 & \Delta u_x \geq \sigma_0/M. \end{cases} \tag{9}$$

Thus, at the crack tip ($x_1 = 0$) we must have

$$\sigma_{zx}(-0) = \sigma_{zx}(+0) = \sigma_0, \tag{10}$$

while at the end of the FPZ ($x_1 = -a$), the traction is zero:

$$\sigma_{zx}(-a) = 0. \tag{11}$$

For $x_1 < -a$ (outside the FPZ), we assume that the shear traction is zero when $|x_1|$ is of order of a. For remote points and/or at infinity there are some external driving forces. For certainty and to compare results with those of *Burridge et al.* [1979], when appropriate, we will assume that the external force is point shear force of intensity P following the crack tip at a constant distance l ($l \gg a$):

$$\sigma_{zx}(x_1) = P\delta(x_1 + l) \text{ for } x_1 < a \tag{12}$$

where $\delta(x)$ is the δ function.

[19] The DD must be finite at $x_1 = -\infty$. We need to find the solution of (7) in the physical plane providing finite DD at $x_1 = -\infty$, satisfying the boundary conditions (8), (12) outside the FPZ, the conditions (9) within it and the conditions (10) and (11) at start and end point of the FPZ, respectively. The solution must give the distribution of the DD, and, through (9), tractions in the FPZ.

2.2. Influence Functions With Singular Traction at the Crack Tip

[20] A solution of the problem –(12) has been actually obtained by *Burridge et al.* [1979]. The authors first derived the influence functions giving a solution of an auxiliary problem, when unit point force ($P = 1$) is applied at an arbitrary point x_0 behind the tip ($x_0 < 0$), while there is no FPZ and, consequently, no conditions (9)–(11). Having a solution of the auxiliary problem, one may multiply it by the density $\sigma_{zx}(x_0)$, integrate with respect to x_0 and use the result in (8)–(11). This gives an integral equation and additional conditions, under which it is to be solved.

[21] *Burridge et al.* [1979] derived a solution (influence functions) for the traction $\Sigma_{zx}(x_1, x_0)$ and for the DD $\Delta U_x(x_1, x_0)$, which give a finite traction at the crack tip ($x_1 = 0$), while the displacements were infinite at $x_1 = -\infty$. Since singularity of the traction was excluded by such a choice, the authors could not use the stress intensity factors (SIFs), even in the case $\gamma = 0.5$ equivalent to a static problem. Here we present another influence function, which has a singular traction at $x_1 = +0$, while the DD are finite at $x_1 = -\infty$. This choice allows us to use the SIFs as generalized characteristics of external loads and it clearly reveals the connection with the classical results of fracture mechanics, in particular, it gives an energy relation used in section 2.3.

[22] Omitting lengthy derivation, involving inversion of (5), we present the final result for the needed influence functions. It is

$$\frac{d\Delta U_x(x_1,x_0)}{dx_1} = \frac{1}{\pi\mu}|C(v)|\left[\sin(\pi\gamma)\left(\frac{x_0}{x_1}\right)^{\gamma}\frac{1}{x_1-x_0} + \pi\cos(\pi\gamma)\delta(x_1-x_0)\right] \quad x_1 \le 0, \tag{13}$$

$$\Sigma_{zx}(x_1,x_0) = -\frac{1}{\pi}\sin(\pi\gamma)\left(\frac{-x_0}{x_1}\right)^{\gamma}\frac{1}{x_1-x_0} \qquad x_1 \ge 0. \tag{14}$$

[23] When $x_1 \to +0$, the singular traction defined by (14) behaves as $\Sigma_{zx}(x_1, x_0) = -[K_{IIu}(x_0)/(2\pi x_1)^{\gamma}]$, where $K_{IIu}(x_0)$ is the SIF generated by unit point force at a point x_0:

$$K_{IIu}(x_0) = -\frac{2\sin(\pi\gamma)}{[2\pi(-x_0)]^{1-\gamma}}. \tag{15}$$

In the case $\gamma = 0.5$, K_{IIu} is a common SIF characterizing the intensity of square-root singularity at the crack tip $x_1 = 0$.

2.3. Eigenvalue Problem for the FPZ: Solution of the Problem

[24] Denote K_{IIe} the SIF generated by external loads; in particular, when the driving force is assumed to be point force (12), we have from (15),

$$K_{IIe} = -\frac{2\sin(\pi\gamma)}{(2\pi l)^{1-\gamma}}P. \tag{16}$$

The SIF, generated by internal forces in the FPZ, is

$$K_{IIi} = \int_{-a}^{0}\sigma_{zx}(x_0)K_{IIu}(x_0)dx_0 = -2\sin(\pi\gamma)\int_{-a}^{0}\sigma_{zx}(x_0)\frac{dx_0}{[2\pi(-x_0)]^{1-\gamma}}.$$

The total traction at $x_1 = 0$, in view of (10), must be finite. Hence the sum of the SIFs turns to zero: $K_{IIe} + K_{IIi} = 0$, and we obtain the condition

$$2\sin(\pi\gamma)\int_{-a}^{0}\sigma_{zx}(x_0)\frac{dx_0}{[2\pi(-x_0)]^{1-\gamma}} = K_{IIe}, \tag{17}$$

defining the size of the FPZ.

[25] By using (13) we find the derivative of the DD:

$$\frac{d\Delta u_x(x_1)}{dx_1} = \frac{1}{\pi\mu}|C(v)|\int_{-\infty}^{0}\sigma_{zx}(x_0)\cdot\left[\sin(\pi\gamma)\left(\frac{x_0}{x_1}\right)^{\gamma}\frac{1}{x_1-x_0} + \pi\cos(\pi\gamma)\delta(x_1-x_0)\right]dx_0 \quad x_1 \le 0.$$

When the external loads are represented by the point force (12), after expressing the force P through (16) and substituting K_{IIe} from (17), we obtain

$$\frac{d\Delta u_x(x_1)}{dx_1} = \frac{|C(v)|}{\mu\pi}\{\sin(\pi\gamma)\cdot\int_{-a}^{0}\left[\left(\frac{x_0}{x_1}\right)^{\gamma}\frac{1}{x_1-x_0} - \frac{1}{(-x_1)}\left(\frac{x_1}{x_0}\right)^{1-\gamma}\right]\cdot\sigma_{zx}(x_0)dx_0 + \pi\cos(\pi\gamma)\sigma_{zx}(x_1)\} \quad x_1 \le 0. \tag{18}$$

[26] Introduce normalized variables $y = -x_1/a$, $\eta = -x_0/a$ and functions

$$G_{1-\gamma}(\eta,y) = \int_0^{\eta/y}\frac{d\xi}{\xi^{1-\gamma}(1-\xi)}, H(\eta/y-1) = \begin{cases} 0 & \eta < y \\ 1 & \eta > y. \end{cases}$$

[27] Then after the change of the variables and integration by parts accounting for the condition (11), we obtain

$$\frac{d\Delta u_x(y)}{dy} = -\frac{a|C(v)|}{\pi\mu}\int_0^1 \left[\sin(\pi\gamma)G_{1-\gamma}(\eta,y) - \pi\cos(\pi\gamma)H(\eta/y-1)\right]\frac{d\sigma_{zx}(\eta)}{d\eta}d\eta \quad y \geq 0. \tag{19}$$

For the FPZ with the linear softening law (9), equation (19) yields the eigenvalue problem

$$\frac{d\Delta u_x}{dy}(y) - \lambda_c(\gamma)\int_0^1 \left[G_{1-\gamma}(\eta,y) - \pi\cot(\pi\gamma)H(\eta/y-1)\right]\cdot\frac{d\Delta u_x}{d\eta}(\eta)d\eta = 0 \qquad 0 \leq y \leq 1, \tag{20}$$

where

$$\lambda_c(\gamma) = \frac{1}{\pi}|C(v)|\frac{Ma}{\mu}\sin(\pi\gamma). \tag{21}$$

The eigenvalues of (20) depend on the rupture velocity through the parameter γ. Since the right-hand side of (21) is positive, only positive eigenvalues of (20) are physically significant. The least positive eigenvalue $\lambda_c(\gamma)$ defines the size of the FPZ:

$$a = \pi\frac{\lambda_c(\gamma)}{\sin(\pi\gamma)|C(v)|}\frac{\mu}{M}. \tag{22}$$

[28] The corresponding eigenfunction after integration with using the conditions (9)–(11) gives the distribution of the DD and tractions in the FPZ. Then, (17) defines the corresponding SIF; and (18) defines the derivative of the DD outside the FPZ. Integration of (18) provides the DD. In the normalized coordinates they are

$$\Delta u_x(y) = -\frac{a|C(v)|}{\pi\mu}\sin(\pi\gamma)\int_0^1 \left[I_{1-\gamma}(y,\eta) + \pi\cot(\pi\gamma)\cdot H(y/\eta-1)\right]\sigma_{zx}(\eta)d\eta \quad y \leq 0,$$

where

$$I_{1-\gamma}(y,\eta) = \int_0^{y/\eta}\frac{\xi^{1-\gamma}d\xi}{1-\xi}.$$

For the points of the FPZ ($0 \leq y \leq 1$) the equation turns into equation (94) by *Burridge et al.* [1979].

[29] By using (14) and the condition (17) we can also find the traction ahead of the tip:

$$\sigma_{zx}(x_1/a) = \frac{\sin(\pi\gamma)}{\pi}\int_0^1 \left(\frac{x_1/a}{\eta}\right)^{1-\gamma}\frac{\sigma_{zx}(\eta)}{\eta + x_1/a}d\eta \quad x_1 \geq 0.$$

This is actually equation (119) by *Burridge et al.* [1979].

[30] Note that when γ tends to zero, equation (20) tends to

$$\frac{d\Delta u_x}{dy}(y) = \xi_c(\gamma)(\Delta u_x - \Delta u_0), \tag{23}$$

where

$$\xi_c(\gamma) = \lambda_c(\gamma)\pi\cot(\pi\gamma), \tag{24}$$

$\Delta u_0 = \sigma_0/M$. Equations (23), (9) and (11) imply that in limit $\gamma \to 0$, the DD behave exponentially as

$$\Delta u/\Delta u_0 = \exp[-\lambda_c\pi\cot(\pi\gamma)(1-y)], \tag{25}$$

near the end of the FPZ $y = 1$. On the other hand, near the crack tip ($y = 0$), the analysis of (20) yields the power type asymptotic:

$$\Delta u/\Delta u_0 = O\left(y^{2-\gamma}\right). \tag{26}$$

This asymptotic holds for any γ.

3. Approximate Versus Exact Solution

3.1. Approximate Approach

[31] Let us write (3) with the complex argument $\Omega = \xi + i\omega$ instead of ω:

$$\frac{d\Delta u_x}{dt}(\Omega) = -\frac{1}{p\mu}C\sigma_{zx}(\Omega). \tag{27}$$

Equation (27) corresponds to using the potentials of plane waves of the form

$$f_c(\Omega,z) = A_c\exp\left(-i\omega\zeta_c\frac{|z|}{c}\right)\exp(\Omega q), \tag{28}$$

where as above $q = t - px$, ς_c is defined by (4) with $c = \alpha$ for the longitudinal wave and $c = \beta$ for the shear wave, $C = |C(v)|\exp(i\pi\gamma\,\mathrm{sgn}\omega)$, and γ is defined by (7).

[32] The function (28) satisfies the wave equation. For the subsonic propagation, it exponentially decreases with the distance from the surface $z = 0$ as

$$\left|\frac{f_c(\Omega,z)}{f_c(\Omega,0)}\right| = \exp\left(-\left|\sqrt{p^2c^2-1}\frac{\omega z}{c}\right|\right), \tag{29}$$

and the corresponding displacements and stresses decrease with the same rate.

[33] Formally use the dependence (9) differentiated with respect to time in the potentials of the form (28). Then after separating real and imaginary parts, equation (27) yields

$$\omega = \frac{1}{p}\frac{M|C(v)|}{\mu}\sin(\pi\gamma), \qquad \xi = \frac{1}{p}\frac{M|C(v)|}{\mu}\cos(\pi\gamma). \tag{30}$$

The wavelength a_w, corresponding to the frequency ω, is $a_w = 2\pi/(|\omega|p)$. We will call it the dominant wavelength. The

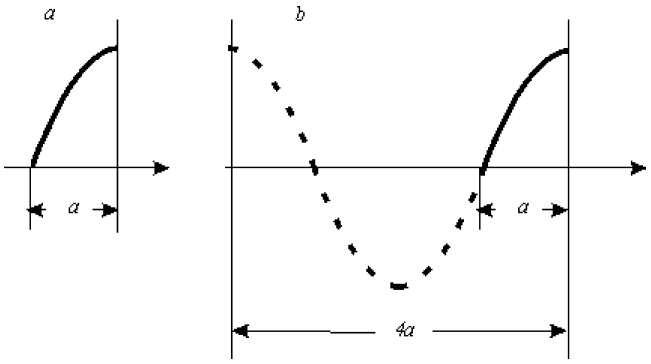

Figure 3. Relation between (a) the size a of the FPZ and (b) the dominant wavelength $a_w \approx 4a$.

corresponding exponent, written in terms of the wavelength, is $\xi_w = \xi a_w p$. By using a_w and ξ_w we may write (30) as

$$\lambda_w(\gamma) = 2, \tag{31}$$

$$\xi_w(\gamma) = \lambda_w(\gamma)\pi \cot(\pi\gamma), \tag{32}$$

where

$$\lambda_w(\gamma) = \frac{1}{\pi}|C(v)|\frac{Ma_w}{\mu}\sin(\pi\gamma). \tag{33}$$

Note that λ_w is similar to λ_c in (21), while ξ_w is similar to ξ_c in (24). This similarity is due to the fact that the pair λ_c, $\lambda_c\cot(\pi\gamma)$ and the pair λ_w, $\lambda_w\cot(\pi\gamma)$ arise from the same multiplier $C = |C(v)| \exp(i\pi\gamma\,\mathrm{sgn}\omega)$ in the starting equations (3) and (27).

3.2. Comparing Approximate and Exact Solutions

[34] From (21), (23), and (31) we have the dependence between the size of the FPZ a and the dominant wavelength a_w:

$$\frac{a}{a_w} = \frac{\lambda_c(\gamma)}{2}, \tag{34}$$

where λ_c is the least positive eigenvalue of (20). Since $\lambda_c(\gamma)$ is known from the solution of (20) and a_w is known from (33), (31), the dependence (34) allows us to evaluate the size of the FPZ in terms of the dominant wavelength for any wave velocity.

[35] Comparing (24) with (32) shows that the amplification exponents differ only by the normalization of distances: ξ_c corresponds to the normalization by a, while ξ_w corresponds to the normalization by a_w. Thus they are actually equivalent. Consider results following from the exact and approximate solutions for various ranges of the propagation velocity.

3.2.1. Subsonic Propagation With $v < v_R$

[36] In this case, $\gamma = 0.5$, and equation (20) turns into that studied by *Linkov* [1978] for the static case ($v = 0$, $|C(0)| = 2(1 - \nu)$) [see also *Petukhov and Linkov*, 1979; *Linkov*, 1994]. In this case, the kernel in (20) is positive definite and it was found that the first eigenvalue is

$$\lambda_c = \frac{1}{\pi}|C(v)|\frac{Ma}{\mu} = 0.4655. \tag{35}$$

On the other hand, the approximate equation (31) gives

$$\lambda_w = \frac{1}{\pi}|C(v)|\frac{Ma_w}{\mu} = 2. \tag{36}$$

From (35), (36) we obtain

$$\frac{a_w}{a} = \frac{2}{\lambda_c} = 4.3 \approx 4. \tag{37}$$

Thus, with accuracy of 7.8%, the dominant wavelength, defined by the approximate approach, equals to fourfold size of the FPZ. In other words, the approximate approach is valid if the size of the FPZ is associated with one fourth of the dominant wavelength. This remarkable correspondence has a natural physical interpretation (Figure 3): In fact, one fourth of a harmonic cycle is exactly that its part, at which softening may occur (the traction decreases from the maximum value to zero).

[37] It was also stated for a static case [*Linkov*, 1978] and for the subsonic crack propagation [*Linkov*, 2005] that the eigenvalue (35) corresponds to the exact energy equation:

$$\frac{1}{4\mu}|C(v)|K_{IIe}^2 = \frac{1}{2}\frac{\sigma_0^2}{M}, \tag{38}$$

which turns into the Griffith criterion in the static case. Since in the considered case $1/|C(v)|$ decreases with growing velocity as shown in Figure 4, (38) implies that the crack propagation is unstable, that is the velocity increases under decreasing external load, characterized by the SIF K_{IIe}. Note that *Burridge et al.* [1979] came to the same conclusion for a particular case of point external load; as mentioned, they did not use SIFs and consequently they did not employ the energy equation (38).

[38] The approximate solution (36), written as

$$\frac{1}{\mu}|C(v)|a_w = \frac{2\pi}{M}, \tag{39}$$

shows that the dominant wavelength decreases with the growing velocity. This means abnormal dispersion. Comparing (38) with (39), we see that the unstable propagation corresponds to abnormal dispersion stated by the approximate approach.

[39] At last, in the considered case, there are no traces of exponential behavior, since for $\gamma = 0.5$ equations (24) and (32) give $\xi_c = \xi_w = 0$.

3.2.2. Subsonic Propagation ($v_R < v < \beta$)

[40] In this case, from (7) it follows that $\gamma = -0.5$. Then the kernel of the equation (20) becomes negative definite. Hence it has only negative eigenvalues and it is impossible to satisfy (21) for softening. There is no exact solution in this case.

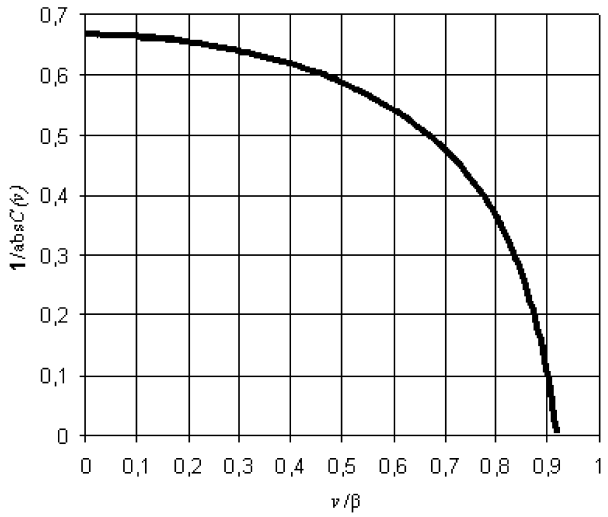

Figure 4. Dependence of $1/|C(v)|$ on the normalized velocity v/β in subsonic range below the Rayleigh velocity ($\nu = 0.25$, $\alpha/\beta = \sqrt{3} = 1.73$, $v_R/\beta = 0.92$).

[41] The approximate approach gives the equation similar to (36):

$$\frac{1}{\pi}|C(v)|\frac{Ma_w}{\mu} = -2. \tag{40}$$

It also cannot be satisfied for (positive) softening modulus M. Thus the conclusion coincides with that of the exact solution: The range of rupture speeds $v_R < v < \beta$ is forbidden.

[42] Note, however, that for elastic interface, we change M to the contact rigidity $1/b$ (Figure 1) taken with the minus sign. Then (40) turns into the dispersion equation for a "slow" interface wave, obtained by *Pyrak-Nolte and Cook* [1987].

3.2.3. Intersonic Propagation ($\beta < v < \alpha$)

[43] First, compare exact and approximate sizes of the FPZ. We calculated the least eigenvalues of (20) with five correct significant digits. Figure 5 presents them as the function of the normalized velocity v/β, when the Poisson ratio is 0.25 ($\alpha/\beta = \sqrt{3} = 1.73$). We see that except for very close vicinity of the shear ($v = \beta$) and longitudinal ($v = \alpha$) velocity, the eigenvalue does not differ significantly from the value $\lambda_c = 0{,}4655$, corresponding to the value $\gamma = 0.5$, discussed above. The difference is less than 8.6% when $1.06 < v/\beta < 1.70$. Hence the result (37) showing that the dominant wavelength approximately equals to fourfold size of the FPZ holds in the main portion of the intersonic region.

[44] Second, consider the exponential behavior (25) of the DD, predicted by both exact and approximate solutions near the end of the FPZ ($y = 1$), when $\gamma \neq 0$. Calculations show that the asymptotic formula (25) does agree with the exact solution. As an example, Figure 6 presents the normalized DD for $\gamma = 0.01$. In this case, the computed eigenvalue is $\lambda_c = 0.05833$, and $\xi_c = \lambda_c \pi \cot(\pi\gamma) = 5.8311$. The curve defined by (25) is indistinguishable from that in Figure 6. The relative error of (25) is less than 1% when $y \geq 0.6$. Note, however, that for smaller values of y ($y \leq 0.3$) the asymptotic equation (25) is not valid, and in accordance with (26) the asymptotic becomes of power type near the crack tip. In this area, the curves are indistinguishable only because of the small absolute values of the DD.

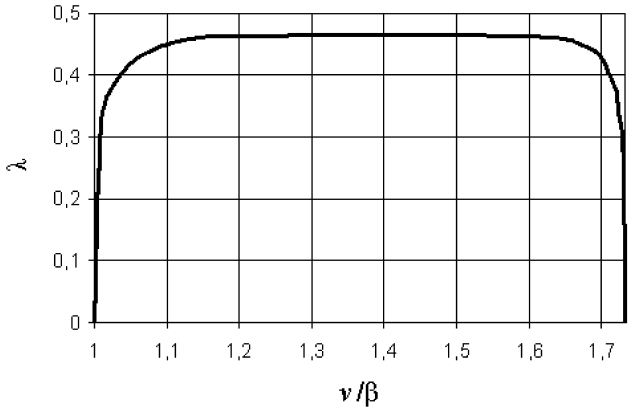

Figure 5. Eigenvalue λ as function of the normalized velocity v/β in intersonic range ($\nu = 0.25$, $\alpha/\beta = \sqrt{3} = 1.73$).

[45] Third, consider stability of the propagation. When $\beta < v \leq \sqrt{2}\beta$, the exact solution for the point external force (12) shows unstable propagation [*Burridge et al.*, 1979]. The approximate solution gives

$$\frac{1}{\pi}|C(v)|\frac{Ma_w}{\mu}\sin(\pi\gamma) = 2. \tag{41}$$

The graph of the function $C(v)\sin(\pi\gamma)$ is presented in Figure 7 for the Poisson's ratio equal to 0.25. Since this function grows in the considered range, (41) implies that the dispersion is abnormal. Hence, again, unstable propagation corresponds to abnormal dispersion stated by the approximate approach.

[46] When $\sqrt{2}\beta < v < \alpha$, the numerical results by *Burridge et al.* [1979] for the external force prescribed by (12) indicate that the propagation is unstable up to some value of the velocity depending on the distance from the applied point force to the crack tip. The motion becomes

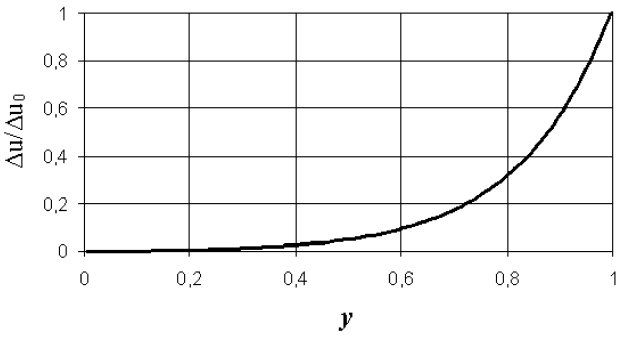

Figure 6. Normalized DD $\Delta u/\Delta u_0$ as function of the normalized distance $y = -x/a$ ($\gamma = 0.01$, $\gamma_c = 0.05833$).

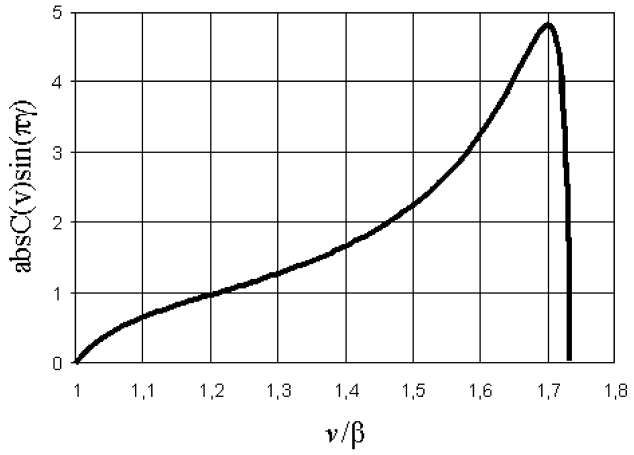

Figure 7. Dependence of $|C(v)|$ on the normalized velocity v/β in intersonic range ($\nu = 0.25$, $\alpha/\beta = \sqrt{3} = 1.73$).

stable when the velocity exceeds this value. In accordance with these results, (41), and the graph of Figure 7 give abnormal dispersion before $v/\beta < 1.7$ and normal dispersion for $1.7 < v/\beta < \sqrt{3}$. Note, however, that *Burridge et al.* [1979] obtained the value v/β, at which unstable propagation changes to stable one, less than 1.7: Its maximal value was 1.51. Still, the graphs given by *Burridge et al.* [1979] show that this value depends on a particular external load, and really significant growth of the external force starts only in the near vicinity of the longitudinal wave velocity, when $v/\beta > 1.7$.

3.2.4. Particular Case of Intersonic Propagation With $v = \sqrt{2}\beta$

[47] In this particular case of the intersonic propagation we have $\gamma = 0.5$. Hence all the results for a static problem are again applicable. In particular, we again conclude that the approximate approach is valid if the size a of the FPZ is associated with one fourth of the dominant wavelength a_w defined by (36). Now $|C(\sqrt{2}\beta)| = 1/\sqrt{1 - 2\beta^2/\alpha^2}$, what slightly exceeds the static value $|C(0)| = 2(1 - \nu)$. In particular, for $\nu = 0.25$, we have $|C(\sqrt{2}\beta)| = \sqrt{3} = 1.73$, while $|C(0)| = 1.5$. Consequently, the size of the FPZ, defined by (35), the dominant wavelength, defined by (36), and the energy release rate, defined by the left-hand side of (38), do not significantly differ from those in the static case.

[48] We see that for all the velocities the results of the approximate approach are in close correlation with those of the exact solution. Recall that in the subsonic region and also in the intersonic region for $v = \sqrt{2}\beta$, the results agree with accuracy to 7.8% when the size of the FPZ is associated with one fourth of the dominant wavelength. As shown, actually, this result holds in the main portion of the intersonic region. Stable (unstable) propagation corresponds to normal (abnormal) dispersion. In the limits $v \to \beta$ and $v \to \alpha$ ($\gamma \to 0$), the both solutions indicate the same exponential amplification of the DD near the end of the FPZ ($y = 1$). Taking into account good quantitative agreement in the subsonic region, we may try to apply the approximate approach to the analysis of the subsonic rupture propagation in the Chi-Chi earthquake.

4. Application to the Chi-Chi Earthquake

[49] It is interesting to validate the theoretical results against data on rupture pulses in earthquakes. However, field data needed are scarce; those available, as the Pacoima Dam strong motion recording, which served for a detailed analysis [e.g., *Trifunac and Hudson*, 1971; *Bolt*, 1972; *Boor and Zoback*, 1974], were obtained from a single station in a close vicinity (0.2–5 km) of a rupture surface. "Except for limited cases, in the past times seismic stations were situated far away from the fault..." [*Wang et al.*, 2002, p. 507].

[50] The 20 September 1999 Chi-Chi, Taiwan, earthquake is actually a unique event, which may serve for a comparison: "Despite the devastating effects of the event, the ground-motion recordings of the Chi-Chi earthquake provide an ideal opportunity for seismologists to investigate the rupture mechanism of a large earthquake from the near-field measurements" [*Chen et al.*, 2001, p. 1247].

4.1. Observed Effects

[51] *Chen et al.* [2001] give important findings, which will serve us for the analysis. Figure 8 reproduces the scheme of this paper. The solid line shows the surface rupture along the Chelungpu fault exposed after the Chi-Chi earthquake. The fault dips at 29° from this line to the east. The star on the scheme denotes the epicenter of the earthquake; the focal depth was about 8 km. The motion in the earthquake was of the thrust type. The rupture propagated from south to north.

[52] Nine stations along the rupture line are within the range of 3.5 km from the rupture surface. Accelograms recorded by these stations, as shown by *Chen et al.* [2001], clearly reveal the conspicuous S_1 phase; it arrived after the longitudinal ($\alpha = 6.0$ km/s) and shear ($\beta = 3.46$ km/s) waves. *Chen et al.* [2001, p. 1251] cogently show that "...the observed S_1 phase is associated with the rupture pulse reaching the surface." The amplitude of the S_1 phase decreased with the distance from the rupture surface; there was no its traces at stations TCU078, TCU079, TCU084 and TCU089 located farther from the surface, although they were close to the epicenter. There were no its traces at the stations TCU071, TCU072 and TCU074, as well; the station TCU071, the closest of them to the rupture surface, was at the distance of some 8 km from the fault surface.

[53] A typical shear displacement graph, obtained by *Chen et al.* [2001] by repeated integration of accelerations recorded for the S_1 phase, is schematically shown in Figure 9 for the station TCU075. For it, the maximum ground displacement is 0.17 m, and the risetime is 3 s. Note that the maximum displacement is close to the permanent offset. This reminds us that the displacement, obtained by a surface element in the FPZ is just a part of the maximal displacement; consequently, the time, during which the element experiences softening within the FPZ, is a part of the risetime. The duration of the S_1 phase was larger near the northern part of the fault. Specifically, for the stations on the footwall, the risetime of recorded displacements increased from approximately $T_{rS} = 2.7$ s in the southern part to

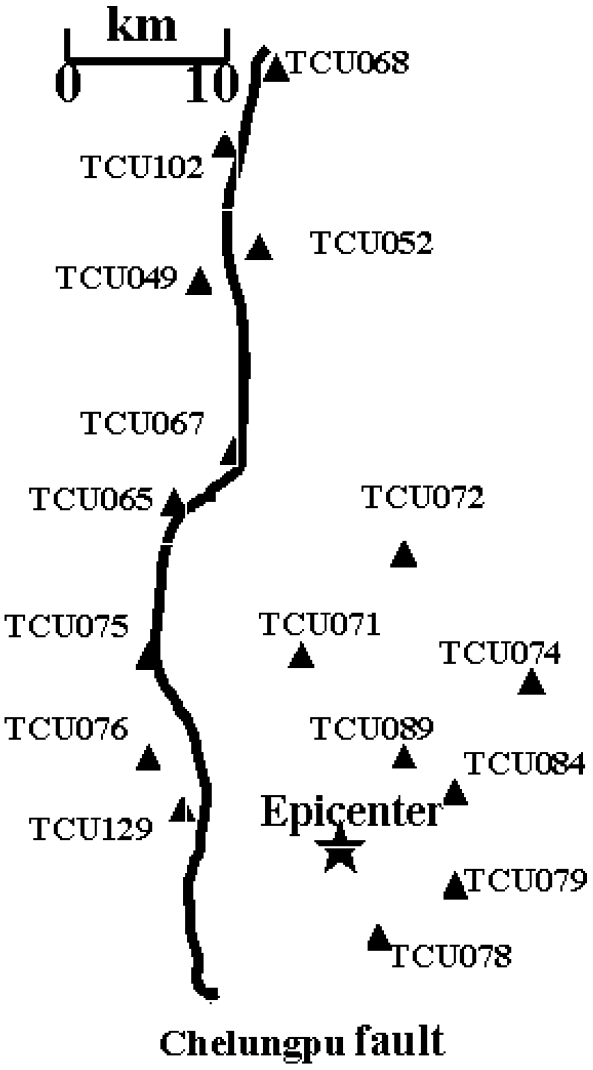

Figure 8. Positions of seismic stations and surface rupture traces caused by the Chi-Chi earthquake.

T_{rN} = 3.8 s in the northern part. The ratio is T_{rN}/T_{rS} = 1.4; the average risetime for the stations on the footwall is T_r = 3.2 s. The velocity of the S_1 phase varied from 2.28 to 2.69 km/s with the average value about 2.49 km/s; it decreased from south to north.

4.2. Application of the Theory

[54] For the interface, we assume that the tractions are connected with the DD by constitutive equations accounting for the fact that the shear strength is finite: After it is reached, a contact element experiences softening. The diagrams "shear traction-shear DD" ($\sigma_{n\tau} - \Delta u_\tau$) are of the type obtained for rocks in experiments by *Barton and Chaubey* [1977]. They are shown in Figure 10 for various values of the normal compressive traction σ_{nn}; the arrow shows the sequence of diagrams, for which $|\sigma_{nn}|$ grows. The points of the maximal shear traction correspond to the shear strength law; in particular, it may be the Coulomb's law: $|\sigma_{n\tau}| = c_0 + |\sigma_{nn}| \tan \rho_0$, where c_0 is the initial cohesion, ρ_0 is the initial friction angle. The descending portions refer to softening (strain weakening) characterized by the softening modulus M. The latter depends on the DD and also on the normal pressure: M decreases with growing $|\sigma_{nn}|$. The horizontal portions of curves correspond to the residual shear strength; the latter also may be of the Coulomb's type: $|\sigma_{n\tau}| = c_* + |\sigma_{nn}| \tan \rho_*$, where c_* is the residual cohesion, ρ_* is the residual friction angle. The normal DD may depend on the shear DD. Constitutive equations, describing these properties and also contact viscosity are given in Appendix A.

[55] In this section, having in mind uncertainty of mechanical parameters for the Chi-Chi earthquake, we will use the simplest approximation. We assume that the initial state of a fault prior to an earthquake is in a vicinity of the maximal shear strength defined by the initial normal pressure. Thus it is described by some of the curves in Figure 10. To further simplify the problem, we approximate the softening portion of this curve by straight segment with the constant softening modulus M. For the shear DD in the rupture process, we neglect the part before the maximal shear strength. Then the diagram becomes of the type shown in Figure 1b. By assuming embedding rock linearly elastic, we may apply superposition and present the shear traction as the sum of the residual and "additional" tractions, and reformulate a problem in terms of the additional quantities. Then, for the additional tractions we arrive at the diagram with zero residual shear strength, described by equations (9). Emphasize that in the analysis of section 2, the superposition influences only external loads, characterized by the SIF K_{IIe}; it does not change the dispersion equation used in the simplified approach.

[56] We also neglect the normal DD on the fault surface and assume that the major shear DD is in the direction of the

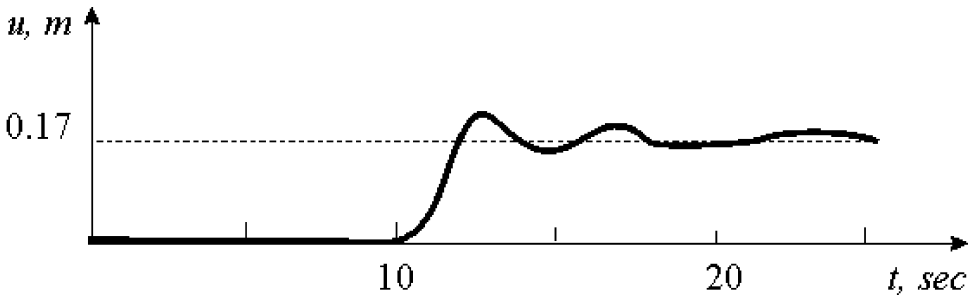

Figure 9. E-W displacement, obtained by repeated integration of acceleration recorded for the conspicuous phase at the station TCU075 [after *Chen et al.*, 2001].

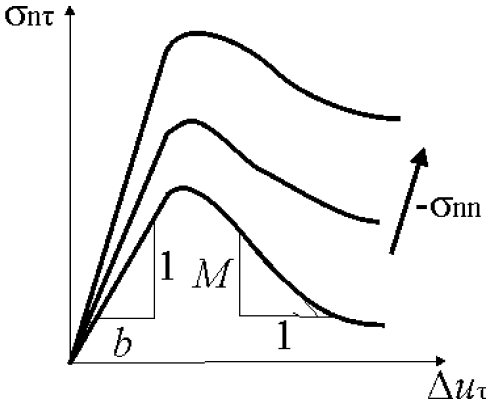

Figure 10. Diagrams of a softening interface. Ascending elastic portions have the compliance b; descending softening portions have the softening modulus M.

rupture propagation. Many of these assumptions may be removed by using the dispersion equation given in Appendix A. We will not do this here because they look less significant that the last one: We neglect the influence of the Earth's surface, which is free of tractions.

[57] Finally, the problem is reduced to that discussed in section 2. Certainly, it is very simplistic. Still, we believe that it may reflect significant features of the rupture pulse in the Chi-Chi earthquake. Indeed, our analysis has started from the suggestion that the length of the FPZ distinctly reveals itself in the Fourier spectrum. Thus the main estimated parameter is of geometrical nature: it is the dominant wavelength, or what is equivalent for quasi-steady propagation, the dominant frequency. This characteristic value defines the distance from the FPZ, at which the information on the rupture pulse is distinguishable. As for any surface wave (for instance, Rayleigh, Stoneley, slow or rapid elastic interface waves), the amplitude exponentially decays with the distance in accordance with equation (29). Hence, if the dominant frequency is estimated by using in (29) the data on the pulse velocity and its decaying with the distance from the rupture surface, it, hopefully, may serve for estimating other parameters. Underline that the theory predicts that due to exponential decreasing with the distance, a rupture pulse becomes practically invisible at distances exceeding some fourfold to fivefold size of the FPZ. This explains why the rupture pulse is recorded only in rear cases: when a station is located in a near vicinity of a rupture surface.

4.3. Comparison With Observations

[58] First, as mentioned, we employ the general equation (29) for the exponential decrease of a pulse with the distance $|z|$ from a rupture surface. For the amplitude of a pulse it gives

$$A = A_c \exp\left(-\sqrt{p^2c^2 - 1}\,|z|\,\frac{|\omega|}{c}\right), \qquad (42)$$

where in the considered case $c = \beta = 3.46$ km/s. Let us use in (42) the rupture velocity $v_x = 2.69$ km/s observed in the southern part of the fault. Since amplitudes A, which are less than $0.1A_c$ are indistinguishable from the influence of α and β waves, we conclude from (29) that the frequencies exceeding $\omega_0 \approx 1.4$ 1/s practically do not penetrate to the distance $|z| = 8$ km. Meanwhile, as shown by *Chen et al.* [2001], at the distance of $|z| = 2$ km the amplitude is still close to that on the fault. This implies that specific information on the rupture zone is carried with the frequency close to $\omega_0 \approx 1.4$ 1/s.

[59] The softening time is $T_S = a/v$. By using (37) we obtain

$$T_S = \frac{1}{4.3}\frac{a_w}{v} = \frac{1}{4.3}\frac{2\pi}{\omega_0},$$

which for $\omega_0 \approx 1.4$ 1/s gives $T_S \approx 0.9$ s. Comparison of this value with the observed risetime in the southern part $T_{rS} = 2.7$ s indicates that the softening time takes approximately one third of the risetime.

[60] The size of the softening zone is $a = vT_S \approx 2.4$ km. Having no direct measurements of this size, note only that a value of order 1 km is considered to be realistic [see, e.g., *Rice*, 1980].

[61] Use the first equation in (30) to evaluate the softening modulus. For the specific density $\rho = 2.5 \times 10^3$ kg/m^3 and the shear wave velocity $\beta = 3.46$ km/s, we have the seismic impedance $Z_\beta = \rho\beta = \mu/\beta = 8.7$ MPa s/m and the shear modulus $\mu = 3 \times 10^4$ MPa. Then by taking the rupture wave velocity $v = 2.69$ km/s and the frequency $\omega_0 \approx 1.4$ 1/s, we obtain $M \approx 8$ MPa/m from the first equation of (30). In practice, this value is quite uncertain. From the data on the stress drop (from 2 to 15 MPa) and accompanying deflections (first meters) in earthquakes, summarized, for instance, by *Rice* [1980] and *Kasahara* [1981], we may roughly estimate M as being of order 5 MPa/m. For the Chi-Chi earthquake, the stress drop $\Delta\tau$ in the southern part was evaluated as some 6 MPa [*Hwang et al.*, 2001; *Huang et al.*, 2001]; the corresponding shear displacement Δu_τ was about 1 m [*Chen et al.*, 2001]. Then $M \sim \Delta\tau/\Delta u_\tau \approx 6$ MPa/m. Note also that the value $M \approx 5$ MPa/m was used in the numerical simulation for the southern part of the Chi-Chi earthquake to obtain the best fit model [*Dalguer et al.*, 2001]. On whole, these estimations agree with the value $M \approx 8$ MPa/m.

[62] At last, assuming the ratio μ/M to be the same in the southern and northern parts of the fault, we may use the first equation of (30) to find the ratio T_{rN}/T_{rS} of the softening times in these parts. For the velocities equal to 2.69 and 2.28 km/s in the southern and the northern parts, respectively, we obtain $T_{SN}/T_{SS} \approx 1.5$. If the softening time is approximately the same portion of the risetime in the southern and northern parts, then $T_{rN}/T_{rS} \approx 1.5$. The latter ratio agrees with the observed ratio $T_{rN}/T_{rS} \approx 1.4$.

4.4. Conclusion

[63] The presented analysis, which tends to avoid solving a boundary value problem by using formally derived dispersion equations, shows that the approximate approach may serve as a simple additional means for studying rupture pulses. We can also see the extreme importance of the softening modulus as an independent

parameter, characterizing both a rupture pulse and the stability of a fault.

Appendix A: Dispersion Equations for the Elasticity-Softening-Creep Model

[64] The approximate approach examined in the paper employs the dispersion equation. A particular form of the latter depends on the elastic properties of half-spaces and also on the properties of an interface. Below we present the dispersion equations for the elasticity-softening-creep (ESC) model, which accounts for elastic, softening and viscous deformations at an interface.

A1. ESC Model of Contact Interaction

[65] To account for softening behavior of an interface, consider diagrams shown in Figure 10. They have ascending elastic portions characterized by the elastic compliance b, points of maximum corresponding to the initial shear strength, descending portions with the softening modulus M and horizontal portions of the residual shear strength (for the latter portion, one may assume $M = 0$).

[66] Time effects are taken into account by joining an element described by diagrams of Figure 10 in series with the Kelvin viscous element. This gives the elasticity-softening-creep (ESC) model shown in Figure A1. It presents the simplest extension of the standard linear solid model differing from the latter in only one respect: After reaching the shear strength, the upper element may experience hardening, or ideal plasticity, or softening.

[67] The constitutive equations for the model are discussed elsewhere [*Linkov*, 2001]. They are

$$\mathbf{K}\Delta u + \boldsymbol{\eta}\frac{d\Delta\mathbf{u}}{dt} = (\mathbf{I}_3 + \mathbf{KB})\sigma + \eta\mathbf{B}\frac{d\boldsymbol{\sigma}}{dt}, \qquad \text{(A1)}$$

where $\boldsymbol{\Delta}\mathbf{u} = \mathbf{u}_1 - \mathbf{u}_2 = (\Delta u_x, \Delta u_z, \Delta u_y)^T$ is the displacement discontinuity; $\boldsymbol{\sigma} = (\sigma_{zx}, \sigma_{zz}, \sigma_{zy})^T$ is the traction vector on the interface; the components of these vectors are in the system of coordinates shown in Figure 2; T stands for transposition; $\mathbf{I}_3$ is the unit 3×3 matrix; $\mathbf{K} = \mathrm{diag}(k_x, k_z, k_y)$ is the rigidity matrix of the springs in the Kelvin element; $\boldsymbol{\eta} = \mathrm{diag}(\eta_x, \eta_z, \eta_y)$ is the viscosity matrix of the dashpots in this element; $\mathbf{B} = \mathbf{B}^e + \mathbf{B}^p$ is the compliance matrix of the upper element in Figure A1 with $\mathbf{B}^e = \mathrm{diag}(b_x, b_z, b_y)$ being its elastic part; $\mathbf{B}^p$ accounts for irreversible displacements; $\mathbf{B}^p = \mathbf{0}$ for purely elastic deformations; for irreversible deformations it is

$$\mathbf{B}^p = \frac{1}{H}\begin{pmatrix} \cos^2\chi & \cos\chi\tan\rho_c & 1/2\sin 2\chi \\ \cos\chi\tan\rho_c & \tan^2\rho_c & \sin\chi\tan\rho_c \\ 1/2\sin 2\chi & \sin\chi\tan\rho_c & \sin^2\chi \end{pmatrix},$$

H is a parameter defining a change in the contact strength: $H > 0$ for hardening, $H = 0$ for ideally plastic contact friction; $H < 0$ for softening; ρ_c is the angle of contact friction in the Coulomb's law: $|\sigma_{n\tau}| = c_c + |\sigma_{nn}|\tan\rho_c$; χ is the angle between the vector of the shear traction in the interface plane ($z = 0$) and the direction of the x axis. We will assume that a contact is isotropic: $k_x = k_y = k$, $\eta_x = \eta_y = \eta$, $b_x = b_y = b$. Then for a softening contact ($H < 0$) the parameter H is defined by the instant softening modulus M as $H = -M/(1 + bM)$ with $-Hb < 1$. Creep acceleration in the ESC model is excluded by inequality $k > M$. The long-term modulus M_∞ is defined by equation $1/M_\infty = 1/M - 1/k$. For elastic unloading, one may apply $H = \infty$.

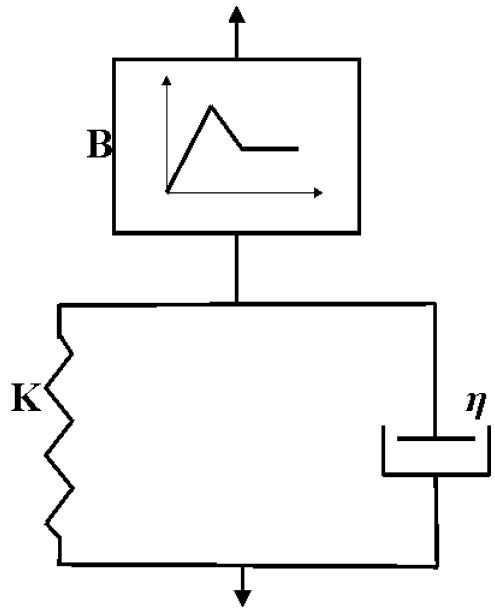

Figure A1. Simplest extension of the standard linear solid model: the elasticity-softening-creep (ESC) model.

[68] In the particular case $\mathbf{B} = \mathbf{0}$, the ESC model reduces to the Kelvin model. For $\mathbf{K} = \mathbf{0}$ we have an extension of the Maxwell model to a contact with irreversible displacements. In the case $\mathbf{K} = \infty$, there is no influence of viscosity: $\boldsymbol{\Delta}\mathbf{u} = \mathbf{B}\boldsymbol{\sigma}$. The same equation follows from (A1) for infinite viscosity ($\boldsymbol{\eta} = \infty$). Similar equation $\boldsymbol{\Delta}\mathbf{u} = \mathbf{B}_0\boldsymbol{\sigma}$ with $\mathbf{B}_0 = \mathbf{B} + \mathbf{K}^{-1}$ corresponds to zero viscosity ($\boldsymbol{\eta} = \mathbf{0}$). Hence the cases $\boldsymbol{\eta} = \mathbf{0}$ and $\boldsymbol{\eta} = \infty$ are actually equivalent: Results for $\boldsymbol{\eta} = \mathbf{0}$ are obtained from those for $\boldsymbol{\eta} = \infty$ by changing $\mathbf{B}$ to $\mathbf{B}_0 = \mathbf{B} + \mathbf{K}^{-1}$. For certainty, when there is no influence of viscosity, we will set $\boldsymbol{\eta} = \infty$.

A2. Characteristic Determinant and Dispersion Equations for the ESC Model

[69] The dispersion equations are obtained by using the potentials of plane waves of the form (28) in the conditions of (1) equilibrium $\boldsymbol{\sigma}_1 = \boldsymbol{\sigma}_2 = \boldsymbol{\sigma}$ and (2) contact interaction $\boldsymbol{\sigma} = \boldsymbol{\sigma}(\boldsymbol{\Delta}\mathbf{u})$ at the interface $z = 0$. They immediately follow from the equations for transmitted and reflected waves by using the formal changes: $\sin\varphi_c$ to pc and $\cos\varphi_c$ to ζ_c, where φ_c is the angle of a wave direction with the normal to the interface; p is the slowness ($p = 1/v$), $c = \alpha_1$ or β_1 for the medium 1, and $c = \alpha_2$ or β_2 for the medium 2; ζ_c is defined similar to (4):

$$\zeta_c = \begin{cases} -\mathrm{isgn}\omega\sqrt{p^2c^2 - 1} & v < c \\ \sqrt{1 - p^2c^2} & v > c. \end{cases}$$

[70] For the ESC model the equations for transmitted and reflected waves are known [*Linkov*, 2001]. After using the mentioned change, they yield the equations for the ampli-

tudes of the potentials at the upper boundary of the interface shown in Figure 2:

$$\mathbf{L}\mathbf{f}_0^+ = \mathbf{0}. \tag{A2}$$

Herein, $\mathbf{L}$ is the matrix:

$$\mathbf{L} = \Omega^2\boldsymbol{\eta}\mathbf{B}\mathbf{A} + \Omega[(\mathbf{I}_3 + \mathbf{K}\mathbf{B})\mathbf{A} + \boldsymbol{\eta}\mathbf{G}_f] + \mathbf{K}\mathbf{G}_f,$$

$\mathbf{f}_0^+ = (f_{P2}, f_{SV2}, f_{SH2})^T$ is the vector of the amplitudes; $\Omega = \xi + i\omega$ is the complex frequency; as above, ξ is the amplification exponent, ω is the real frequency; $\boldsymbol{\eta}$, $\mathbf{K}$, $\mathbf{B}$ and $\mathbf{I}_3$ are matrices defined for the ESC model; the matrices $\mathbf{A}$ and $\mathbf{G}_f$ depend on the elastic properties of the half-spaces 1 and 2:

$$\mathbf{A} = \begin{pmatrix} \mathbf{R}_2 & \mathbf{0} \\ \mathbf{0}^T & t_2 \end{pmatrix}, \quad \mathbf{G}_f = \begin{pmatrix} \mathbf{S}_1\mathbf{R}_1^{-1}\mathbf{R}_2 + \mathbf{S}_2 & \mathbf{0} \\ \mathbf{0}^T & t_2/t_1 + 1 \end{pmatrix},$$

where $\mathbf{0}$ is 2×1 zero column vector,

$$\mathbf{S}_1 = \begin{pmatrix} \alpha_1 p & \zeta_{\beta 1} \\ \zeta_{\alpha 1} & -\beta_1 p \end{pmatrix}, \quad \mathbf{S}_2 = \begin{pmatrix} \alpha_2 p & \zeta_{\beta 2} \\ -\zeta_{\alpha 2} & \beta_2 p \end{pmatrix},$$

$$\mathbf{R}_1 = Z_{\beta 1}\begin{pmatrix} 2\beta_1 p\zeta_{\alpha 1} & 1 - 2\beta_1^2 p^2 \\ (\alpha_1/\beta_1)(1 - 2\beta_1^2 p^2) & -2\beta_1 p\zeta_{\beta 1} \end{pmatrix},$$

$$\mathbf{R}_2 = Z_{\beta 2}\begin{pmatrix} 2\beta_2 p\zeta_{\alpha 2} & 1 - 2\beta_2^2 p^2 \\ -(\alpha_2/\beta_2)(1 - 2\beta_2^2 p^2) & 2\beta_2 p\zeta_{\beta 2} \end{pmatrix},$$

$t_i = t_i = Z_{\beta i}\zeta_{\beta i}$, $Z_{\beta i} = \mu_i/\beta_i$ is the seismic impedance of shear waves for the medium i (i = 1, 2).

[71] Nontrivial solutions of (A2) exist when the determinant $\Delta(\Omega) = \det \mathbf{L}$ equals zero:

$$\Delta(\Omega) = \det\left\{\Omega^2\boldsymbol{\eta}\mathbf{B}\mathbf{A} + \Omega[(\mathbf{I}_3 + \mathbf{K}\mathbf{B})\mathbf{A} + \boldsymbol{\eta}\mathbf{G}_f] + \mathbf{K}\mathbf{G}_f\right\} = 0. \tag{A3}$$

Since the determinant is of third-order, equation $\Delta(\Omega) = 0$ is of sixth power in Ω. Hence it has six roots, which may include zero and multiple roots. Each of nonzero roots gives a dependence between the velocity $v = 1/p$, the exponent ξ and the real frequency ω. A nonzero root of (A3), being used in (A2), gives an eigenvector (mode). For a reversible process at a contact, the corresponding solution of (A2) defines an interface wave. For irreversible deformations at a contact, we may associate a solution with a pulse propagating along the interface. In the general case, the roots of (A3) are found numerically by using, for instance, Muller's iterations (see, e.g., G. Korn and T. Korn). In two particular cases, there exist analytical solutions.

A3. Dispersion Equations for a Contact With $\rho_c = 0$, $\chi = 0$ Between Media With Same Properties

[72] Consider elastic media with same properties ($\alpha_1 = \alpha_2 = \alpha$, $\beta_1 = \beta_2 = \beta$, $Z_{\beta 1} = Z_{\beta 2} = Z_\beta$). Assume also that the interface has zero angle of contact friction ($\rho_c = 0$) and the maximum shear traction has the direction of the x axis ($\chi = 0$). Then the matrix $\mathbf{B}$ is diagonal and the system of equations for eigenvectors disintegrates into three independent equations corresponding to the axes x, z and y. Consequently, the roots of the characteristic determinant are found from three independent square equations. Introduce the normalized values: $\Omega_x = \Omega Z_\beta |B_{11}|$ for the first of them, $\Omega_z = \Omega Z_\alpha B_{22}$ for the second, and $\Omega_y = \Omega Z_\beta B_{33}$ for the third, where $B_{11} = b + 1/H$, $B_{22} = b_z$, $B_{33} = b$. Then

$$\Omega_i^{\pm} = -a_i \pm \sqrt{a_i^2 - c_i}, \qquad (i = x, z, y),$$

where

$$a_x = \frac{1}{2}\mathrm{sgn}H\left[(1 + kB_{11})\frac{Z_\beta}{\eta} + \frac{2\zeta_\beta}{\Delta_R}\right], \quad c_x = kB_{11}\frac{Z_\beta}{\eta}\frac{2\zeta_\beta}{\Delta_R},$$

$$a_z = \frac{1}{2}\left[(1 + k_z B_{22})\frac{Z_\alpha}{\eta_z} + \frac{2\zeta_\alpha}{\Delta_R}\right], \quad c_z = kB_{22}\frac{Z_\beta}{\eta_z}\frac{2\zeta_\alpha}{\Delta_R},$$

$$a_y = \frac{1}{2}\left[(1 + k_z B_{33})\frac{Z_\beta}{\eta} + \frac{2}{\zeta_\beta}\right], \quad c_y = kB_{33}\frac{Z_\beta}{\eta}\frac{2}{\zeta_\beta},$$

$$\Delta_R = 4\frac{\beta}{\alpha}p^2\beta_\beta^2\zeta_\beta\zeta_\alpha + \left(2p^2\beta^2 - 1\right)^2.$$

[73] In the special case when there is no influence of viscosity ($\eta = \eta_z = \infty$), one of the roots is zero, while the other equals $-2a_i$. For elastic interaction ($\mathrm{sgn}H > 0$, $B_{11} = B_{33} = b$, $B_{22} = b_z$), the latter gives the dispersion equations for slow and rapid interface waves studied by *Pyrak-Nolte and Cook* [1987]. For a softening contact ($\mathrm{sgn}H < 0$, $|B_{11}| = 1/M$), it gives (30).

A4. Dispersion Equations for a Contact Without Influence of Viscosity Between Media With Different Properties

[74] Consider media 1 and 2, which may have different elastic properties. Neglect the influence of viscosity ($\eta = \eta_z = \infty$); in this case the ESC model (Figure A1) contains only the upper element. Assume also that the maximum shear traction has the direction of the x axis ($\chi = 0$). Then equation for the *SH* component separates from those for the *P* and *SV* components. The characteristic equation for *P* and *SV* components becomes

$$\det\left(\mathbf{C} + \mathrm{sgn}H\frac{1}{\Omega_H}\mathbf{I}_2\right) = 0, \tag{A4}$$

where $\Omega_H = \Omega Z_{\beta 2}/|H|$, $\mathbf{C} = \frac{1}{Z_{\beta 2}}\mathbf{B}_n\mathbf{D}^{-1}$, $\mathbf{D} = \mathbf{S}_1\mathbf{R}_1^{-1} + \mathbf{S}_2\mathbf{R}_2^{-1}$,

$$\mathbf{B}_n = \begin{pmatrix} Hb + 1 & \tan\rho_c \\ \tan\rho_c & Hb_z + \tan^2\rho_c \end{pmatrix},$$

$\mathbf{I}_2$ is the 2×2 unit matrix, and the matrices $\mathbf{S}_1$, $\mathbf{S}_2$, $\mathbf{R}_1$, $\mathbf{R}_2$ are defined above.

[75] The roots of (A4) are

$$\left(\frac{1}{\Omega_H}\right)^{\pm} = -\frac{1}{2}\mathrm{sgn}H(c_{11} + c_{22}) \pm \sqrt{\frac{1}{4}(c_{11} + c_{22})^2 - \Delta_c}, \tag{A5}$$

where

$$c_{11}+c_{22}=\frac{1}{Z_{\beta 2}\Delta_D}\left[d_{22}(Hb+1)+d_{11}\left(Hb_z+\tan^2\rho_c\right)\right],$$
$$\Delta_c=\frac{\Delta_B}{Z_{\beta 2}\Delta_D},$$
$$\Delta_B=\det\mathbf{B}_n=(Hb+1)Hb_z+Hb\tan^2\rho_c,$$
$$\Delta_D=\det\mathbf{D}=d_{11}d_{22}+d_{12}^2,$$
$$d_{11}=\frac{\zeta_{\beta 1}}{Z_{\beta 1}\Delta_{R1}}+\frac{\zeta_{\beta_2}}{Z_{\beta 2}\Delta_{R2}},$$
$$d_{12}=-d_{21}=-\frac{(\beta_1/\alpha_1)a_1}{Z_{\beta 1}\Delta_{R1}}+\frac{(\beta_2/\alpha_2)a_2}{Z_{\beta 2}\Delta_{R2}},$$
$$d_{22}=\frac{(\beta_1/\alpha_1)\zeta_{\beta 1}}{Z_{\beta 1}\Delta_{R1}}+\frac{(\beta_2/\alpha_2)\zeta_{\beta_2}}{Z_{\beta 2}\Delta_{R2}},$$
$$a_j=2p\beta\zeta_{\alpha j}\zeta_{\beta j}+p\alpha_j\left(2p^2\beta_j^2-1\right),$$
$$\Delta_{Rj}=4\left(\beta_j/\alpha_j\right)p^2\beta_j^2\zeta_{\alpha j}\zeta_{\beta j}+\left(2p^2\beta_j^2-1\right)^2,\quad(j=1,2).$$

[76] For the subsonic propagation ($p\beta_1>1$, $p\beta_2>1$) we have

$$d_{11}=-i\ \mathrm{sgn}\omega\left(\frac{\sqrt{p^2\beta_1^2-1}}{Z_{\beta 1}\Delta_{R1}}+\frac{\sqrt{p^2\beta_2^2-1}}{Z_{\beta 2}\Delta_{R2}}\right),$$
$$d_{22}=-i\ \mathrm{sgn}\omega\left(\frac{(\beta_1/\alpha_1)\sqrt{p^2\alpha_1^2-1}}{Z_{\beta 1}\Delta_{R1}}+\frac{(\beta_2/\alpha_2)\sqrt{p^2\alpha_2^2-1}}{Z_{\beta 2}\Delta_{R2}}\right),$$
$$a_j=-2p\beta_j\sqrt{p^2\alpha_j^2-1}\sqrt{p^2\beta_j^2-1}+p\alpha_j\left(2p^2\beta_j^2-1\right),$$
$$\Delta_{Rj}=-4\left(\beta_j/\alpha_j\right)p^2\beta_j^2\sqrt{p^2\alpha_j^2-1}\sqrt{p^2\beta_j^2-1}+\left(2p^2\beta_j^2-1\right)^2,\quad(j=1,2).$$

[77] Now the sum $c_{11}+c_{22}$ is purely imaginary, while the coefficient Δ_c is real. Then an analysis of the solution (A5) leads to the following cases:

[78] 1. If $\Delta_c>0$, there exists only one mode; it propagates with a constant amplitude ($\xi=\mathrm{Re}\Omega=0$).

[79] 2. If $\Delta_c=0$, then one mode, propagating with a constant amplitude ($\xi=\mathrm{Re}\Omega=0$), exists only under the condition

$$\mathrm{sgn}\ H\ \mathrm{sgn}\omega\ \mathrm{Im}(c_{11}+c_{22})>0. \tag{A6}$$

[80] 3. If $\Delta_c<0$ and (A6) is met, there are two modes; their properties are defined by the sign of the discriminant:

$$d=1/4(c_{11}+c_{22})^2-\Delta_c. \tag{A7}$$

(1) If $d>0$, then one of the modes amplifies ($\xi=\mathrm{Re}\Omega>0$), while the other decays ($\xi=\mathrm{Re}\Omega<0$) with the same $|\xi|$ for the same real frequency $\omega=\mathrm{Im}\Omega$, and (2) if $d<0$, the both modes propagate without amplification ($\xi=\mathrm{Re}\Omega=0$).

[81] 4. If $\Delta_c<0$, while (A6) is not satisfied, there are no subsonic modes.

[82] For revealing the influence of the difference in media properties, it looks useful to consider the case, when the media 1 is a rigid wall ($Z_{\beta 1}/Z_{\beta 2}=\infty$). Then the quantities entering equation (A5) in the case of the subsonic propagation are

$$c_{11}+c_{22}=-i\ \mathrm{sgn}\omega\frac{1}{\Delta_{S2}}\left[(Hb+1)\sqrt{p^2\alpha_2^2-1}+\frac{\alpha_2}{\beta_2}\left(Hb_z+\tan^2\rho_c\right)\sqrt{p^2\beta_2^2-1}\right],$$
$$\cdot\ \Delta_c=\frac{\alpha_2}{\beta_2}\frac{1}{\Delta_{S2}}\Delta_B\Delta_{R2},$$

where $\Delta_{S2}=p^2\alpha_2\beta_2-\sqrt{p^2\alpha_2^2-1}\sqrt{p^2\beta_2^2-1}$. Note that $\Delta_{S2}>0$ for physically significant values of p, α_2 and β_2; Δ_B and Δ_{R2} are defined above; equation $\Delta_{R2}=0$ defines the Rayleigh wave velocity v_{R2} of the medium 2. For a softening contact ($H<0$), inequality (A6) is satisfied and $\Delta_B<0$.

[83] The sign of Δ_c depends on the sign of Δ_{R2}. In the range $\beta_2>v_x>v_{R2}$, we have $\Delta_{R2}>0$, what implies $\Delta_c<0$. Hence we have the case 3: There are two modes. They are quite different depending on the sign of d, defined by (A7). A detailed analysis shows that for $\beta_2>v_x>v_{R2}$ the dispersion is normal and weak; for $v_{R2}>v_x$ the dispersion is abnormal. The dispersion curve has a corner point at $v_x/\beta_2=0.933$. It corresponds to a change of the sign of the discriminant d (A7). In the interval $1>v_x/\beta_2>0.933$, we have $d>0$ and in accordance with case 3, mode 1, there are two modes: One of them exponentially amplifies at the end of the FPZ, while the other decays with the same absolute value of ξ. For $0.933>v_x/\beta_2>v_{R2}/\beta_2$, the discriminant d being negative, we have case 3, mode 2. There are still two modes but both of them propagate without exponential growth ($\xi=0$).

[84] Below the Rayleigh velocity ($0<v_x<v_{R2}$), we have $\Delta_{R2}<0$, what implies $\Delta_c>0$. Then, in accordance with case 1, there is only one mode; its amplification exponent is zero. The dispersion in this range is strong and abnormal.

[85] The choice between modes is beyond the dispersion analysis: It requires additional physical considerations or numerical solving of a boundary value problem with initial conditions. Meanwhile, the analysis gives a notion on difficulties, which may arise when trying to numerically find a solution.

[86] **Acknowledgments.** The author gratefully acknowledges the support of the Russian Fund of Fundamental Researches (03-05-64888) at the starting stage of the work concerning the subsonic crack propagation. The results were extended into the intersonic range, and the work was finalized during a 2 month stay at the Division of Applied Mathematics of the University of Liverpool under the support of the EU Marie Curie grant MTKD-CT-2004-509809. The author highly appreciates this support and the friendly help of colleagues at the University of Liverpool.

References

Aki, K., and P. G. Richards (1960), *Quantitative Seismology*, W. H. Freeman, New York.

Andrews, D. (1976), Rupture velocity of plane-strain shear cracks, *J. Geophys. Res.*, *81*, 5679–5687.

Andrews, D. (1985), Dynamic plane-strain rupture with a slip-weakening friction law calculated by a boundary integral method, *Bull. Seismol. Soc. Am.*, *75*, 1–21.

Barton, N. R., and V. Chaubey (1977), The shear strength of rock in theory and practice, *Rock Mech.*, *10*, 1–34.

Bolt, B. A. (1972), San Fernando rupture mechanism and the Pacoima strong-motion record, *Bull. Seismol. Soc. Am.*, *62*, 1053–1061.

Boor, D. M., and M. D. Zoback (1974), Two-dimensional kinematic fault modeling of the Pacoima Dam strong-motion recordings of the February 9, 1971, San Fernando earthquake, *Bull. Seismol. Soc. Am.*, *64*, 555–570.

Burridge, B., G. Conn, and L. Freund (1979), The stability of a rapid mode II shear crack with finite cohesive traction, *J. Geophys. Res.*, *84*, 2210–2222.

Chen, K.-C., B. S. Huang, J.-H. Wang, W.-G. Huang, T.-M. Chang, R.-D. Hwang, H. C. Chiu, and C.-C. P. Tsai (2001), An observation of rupture pulses of the 20 September 1999 Chi-Chi, Taiwan, earthquake from near-field seismograms, *Bull. Seismol. Soc. Am.*, *91*, 1247–1254.

Cook, N. G. W. (1965), A note on rockbursts considered as a problem of stability, *J. S. Afr. Inst. Min. Metall.*, *65*, 437–446.

Crouch, S. L., and C. Fairhurst (1974), Mechanics of coal mine bumps, *Trans. Soc. Min. Eng.*, *256*, 317–324.

Dalguer, L. A., K. Irikura, J. D. Riera, and H. C. Chiu (2001), The importance of the dynamic source effects on strong ground motion during the 1999 Chi-Chi, Taiwan, earthquake: Brief interpretation of the damage distribution on buildings, *Bull. Seismol. Soc. Am.*, *91*, 1112–1127.

Day, S. M. (1982), Three-dimensional simulation of spontaneous rupture: The effect of nonuniform prestress, *Bull. Seismol. Soc. Am.*, *72*, 1881–1902.

Fukuyama, E., and R. Madariaga (1998), Rupture dynamics of a planar fault in a 3D elastic medium: Rate- and slip-weakening friction, *Bull. Seismol. Soc. Am.*, *88*, 1–17.

Galin, L. (1953), *Contact Problems of Elasticity Theory* (in Russian), Gostehizdat, Moscow.

Harris, R. A., and S. M. Day (1999), Dynamic 3D simulation of earthquakes on en echelon faults, *Geophys. Res. Lett.*, *26*, 2089–2092.

Huang, W.-G., J.-H. Wang, B.-S. Huang, K.-C. Chen, T.-M. Chang, R.-D. Hwang, H.-C. Chiu, and C.-C. P. Tsai (2001), Estimates of some parameters for the 1999 Chi-Chi, Taiwan, earthquake based on Brune's source model, *Bull. Seismol. Soc. Am.*, *91*, 1190–1198.

Hwang, R.-D., J.-H. Wang, B.-S. Huang, K.-C. Chen, W.-G. Huang, T.-M. Chang, H. C. Chiu, and C.-C. P. Tsai (2001), Estimates of stress drop at the Chi-Chi, Taiwan, earthquake of 20 September 1999 from near-field seismograms, *Bull. Seismol. Soc. Am.*, *91*, 1158–1166.

Ida, Y. (1972), Cohesive force across the tip of a longitudinal shear crack and Griffith's specific surface energy, *J. Geophys. Res.*, *77*, 3796–3805.

Kasahara, K. (1981), *Earthquake Mechanics*, Cambridge Univ. Press, New York.

Korn, G. A., and T. M. Korn (1968), *Mathematical Handbook*, 2nd ed., McGraw-Hill, New York.

Linkov, A. M. (1978), On the determination of the abutment pressure and evaluation of stability of seam edges accounting for post-failure deformations, *Sov. Min. Sci.*, *14*, 3–7.

Linkov, A. M. (1994), *Dynamic Phenomena in Mines and the Problem of Stability*, 1799 pp., Int. Soc. for Rock Mech., Lisbon, Portugal.

Linkov, A. M. (2001), On amplification of seismic waves near disturbances, *J. Min. Sci.*, *37*, 225–239.

Linkov, A. M. (2005), The size of the end zone and the propagation velocity of a displacement jump, *J. Appl. Math. Mech.*, *69*, 135–140.

Linkov, A. M., and R. J. Durrheim (1998), Velocity amplification considered as a phenomenon of elastic energy release due to softening, in *Proceedings 3rd International Conference on Mechanics of Jointed and Faulted Rock*, edited by H.-P. Rossmanith, pp. 243–248, A. A. Balkema, Brookfield, Vt.

Muskhelishvili, N. (1975), *Some Basic Problems of the Mathematical Theory of Elasticity*, Noordhoff, Groningen, Germany.

Oglesby, D. D., and S. M. Day (2001), Fault geometry and the dynamics of the 1999 Chi-Chi (Taiwan) earthquake, *Bull. Seismol. Soc. Am.*, *91*, 1099–1111.

Ohnaka, M., and Y. Kuwahara (1990), Characteristic features of local breakdown near a crack tip in the transitional zone from nucleation to unstable rupture during stick-slip shear failure, *Tectonophysics*, *175*, 197–220.

Olsen, K., R. Madariaga, and R. Archuleta (1997), Three-dimensional dynamic simulation of the 1992 Landers earthquake, *Science*, *278*, 834–838.

Petukhov, I., and A. Linkov (1979), The theory of post-failure deformations and the problem of stability in rock mechanics, *Int. J. Rock Mech. Min. Sci. Geomech. Abstr.*, *16*, 57–76.

Pyrak-Nolte, L. J., and N. G. W. Cook (1987), Elastic interface waves along a fracture, *Geophys. Res. Lett.*, *14*, 1107–1110.

Rice, J. (1980), The mechanics of earthquake rupture, in *Physics of the Earth's Interior*, *Proc. Int. Sch. Phys. Enrico Fermi*, *78*, edited by A. M. Dziewonski and E. Boschi, pp. 555–649, Elsevier, New York.

Slepyan, L. I. (2002), *Models and Phenomena in Fracture Mechanics*, Springer, New York.

Trifunac, M. D., and D. E. Hudson (1971), Analysis of the Pacoima Dam accelerogram: San Fernando, California, earthquake of 1971, *Bull. Seismol. Soc. Am.*, *61*, 1393–1411.

Wang, J.-H., M.-W. Huang, and K.-C. Chen (2002), Aspects of characteristics of near-field ground motion of the 1999 Chi-Chi (Taiwan) earthquake, *J. Chin. Inst. Eng.*, *25*, 507–519.

A. M. Linkov, Department of Mathematics, Rzeszow University of Technology, 8 ul. Powstancow Warszawy, Rzeszow, 35-959, Poland. (linkoval@prz.rzeszow.pl)